

Article

Half Metallic Ferromagnetism and Transport Properties of Zinc Chalcogenides ZnX_2Se_4 ($X = Ti, V, Cr$) for Spintronic Applications

Mohsen Al-Qhtani ¹, Ghulam M. Mustafa ^{2,*}, Nasheeta Mazhar ³, Sonia Bouzgarrou ^{4,5}, Qasim Mahmood ^{6,7,*}, Abeer Mera ^{8,9}, Zaki I. Zaki ¹, Nasser Y. Mostafa ^{1,†}, Saad H. Alotaibi ¹ and Mohammed A. Amin ¹

- ¹ Materials Science and Engineering Group, Department of Chemistry, Faculty of Science, Taif University, Taif 21944, Saudi Arabia; mohsen@tu.edu.sa (M.A.-Q.); zakimohamed2000@yahoo.com (Z.I.Z.); nmost69@yahoo.com (N.Y.M.); s.alosaimi@tu.edu.sa (S.H.A.); Mohamed@tu.edu.sa (M.A.A.)
- ² Department of Physics, Division of Science & Technology, University of Education, Lahore 54000, Pakistan
- ³ Department of Physics, University of Lahore, Lahore 05422, Pakistan; nasheen@gmail.com
- ⁴ Laboratoire de Microélectronique et Instrumentation (UR 03/13–04), Faculté des Sciences de Monastir, Avenue de l'Environnement, Monastir 5000, Tunisia; b_sona3@yahoo.fr
- ⁵ Department of Physics, College of Science, Qassim University, P.O. Box 64, Buraydah 51452, Saudi Arabia
- ⁶ Basic and Applied Scientific Research Center, Imam Abdulrahman Bin Faisal University, P.O. Box 1982, Dammam 31441, Saudi Arabia
- ⁷ Department of Physics, College of Science, Imam Abdulrahman Bin Faisal University, P.O. Box 1982, Dammam 31441, Saudi Arabia
- ⁸ Department of Physics, College of Arts and Science, Prince Sattam Bin Abdulaziz University, Wadi Addawasir 11991, Saudi Arabia; abeer.mera047@gmail.com
- ⁹ Department of Physics, Faculty of Science, Kafrelsheikh University, Kafrelsheikh 33516, Egypt
- * Correspondence: ghulam.mustafa@phys.uol.edu.pk (G.M.M.); qmmustafa@iau.edu.sa (Q.M.)
- † Current address: Department of Chemistry, Faculty of Science, Suez Canal University, Ismailia 41522, Egypt.



Citation: Al-Qhtani, M.; Mustafa, G.M.; Mazhar, N.; Bouzgarrou, S.; Mahmood, Q.; Mera, A.; Zaki, Z.I.; Mostafa, N.Y.; Alotaibi, S.H.; Amin, M.A. Half Metallic Ferromagnetism and Transport Properties of Zinc Chalcogenides ZnX_2Se_4 ($X = Ti, V, Cr$) for Spintronic Applications. *Materials* **2022**, *15*, 55. <https://doi.org/10.3390/ma15010055>

Academic Editor: In-Sang Yang

Received: 23 November 2021

Accepted: 17 December 2021

Published: 22 December 2021

Corrected: 30 March 2022

Publisher's Note: MDPI stays neutral with regard to jurisdictional claims in published maps and institutional affiliations.



Copyright: © 2021 by the authors. Licensee MDPI, Basel, Switzerland. This article is an open access article distributed under the terms and conditions of the Creative Commons Attribution (CC BY) license (<https://creativecommons.org/licenses/by/4.0/>).

Abstract: In ferromagnetic semiconductors, the coupling of magnetic ordering with semiconductor character accelerates the quantum computing. The structural stability, Curie temperature (T_c), spin polarization, half magnetic ferromagnetism and transport properties of ZnX_2Se_4 ($X = Ti, V, Cr$) chalcogenides for spintronic and thermoelectric applications are studied here by density functional theory (DFT). The highest value of T_c is perceived for $ZnCr_2Se_4$. The band structures in both spin channels confirmed half metallic ferromagnetic behavior, which is approved by integer magnetic moments (2, 3, 4) μ_B of Ti, V and Cr based spinels. The HM behavior is further measured by computing crystal field energy $\Delta E_{crystal}$, exchange energies $\Delta_x(d)$, $\Delta_x(pd)$ and exchange constants ($N_o\alpha$ and $N_o\beta$). The thermoelectric properties are addressed in terms of electrical conductivity, thermal conductivity, Seebeck coefficient and power factor in within a temperature range 0–400 K. The positive Seebeck coefficient shows p-type character and the PF is highest for $ZnTi_2Se_4$ (1.2×10^{11} W/mK²) among studied compounds.

Keywords: Zn based chalcogenides; density functional theory; half metallic ferromagnetism; transport properties

1. Introduction

The continuous increasing demand of data storage devices in the current scenario has triggered the scientific community to exploit materials in having additional degrees of freedom. Therefore, advanced technology demands highly modern devices with reduce sizes and better efficiency. A few decades ago, the coupling of spin of electrons with its charge laid the basis for new debate among scientists and engineers across the globe, giving rise to an emerging field of spintronics [1,2]. This concept modernized quantum computing based on fast speed computers by calculating the spin current in spin up and spin down channels separately instead of charge in conventional electronics. Therefore, it

accelerates the data processing speed and enhances the data storage capability of spintronic devices. This effect of combining of spin with charge of electrons led to the reduction in size, improvement in efficiency and enhanced the non-volatility of solid-state devices [3–5].

The developing concept of half metallic ferromagnetism reorganized the spintronic industry and performance, playing a critical role in devices such as magneto-resistive random-access memory (MRAM), quantum computing, read head of magnetic hard drive, magnetic sensors, spin valves and giant magneto-resistive effect (GMR) [6,7]. Half metallic ferromagnets (HMF) show a conducting behavior in one spin channel while semiconducting or insulating in other. Therefore, due to the presence of gap at Fermi level in one spin channel, the density of states at Fermi level must be 100% spin polarized. Initially, the concept of HMF was launched by de-Groot et al. [8,9] in half-Heusler alloys. Later, it was explored experimentally as well as theoretically in a variety of materials. Theoretically, HMF was examined in pure and doped transition metals, double perovskites and Heusler alloys [10–12]. The Zn based spinel chalcogenides are incipient as a new candidate for spintronic because of their high temperature half metallic ferromagnetic (HMF) behavior.

The main challenges in the fabrication of spintronic devices include the existence of ferromagnetism at low temperature and phase instability at high temperature (RT). According to previous investigations, the origin of half metallic ferromagnetism is still unclear i.e., either it occurs due to spin of electrons or due to accumulation of the magnetic ions [13,14]. Previously, many reports claimed that half metallic ferromagnetism originates from grouping of magnetic ions and secondary phases. To resolve this issue, much work is carried out by doping the non-magnetic elements into the non-magnetic alloys that improved our understanding regarding quantum mechanical states in real materials, which enhance the data storage capability of the spintronic devices. Since the digital information is recorded in terms of binary states of 0 and 1, which represents the spin up and spin down states here. In one spin channel there exists a gap at Fermi level while for other spin channels, it behaves like conductors. [15,16].

In the recent past, extensive research has been carried out on optoelectronic, magnetic and thermoelectric properties of spinel chalcogenides. The single crystal of ZnFe_2S_4 has been grown experimentally for electronic and optical properties which has promising applications [17]. The spinels XCr_2Z_4 ($\text{X} = \text{Zn, Cd, Hg}$; $\text{Z} = \text{S, Se}$) show different phases at variant pressures. The careful analysis of XRD, and Raman spectroscopic on ZnCr_2S_4 confirm the two structural transitions at 22 GPa (I41/amd phase) and 33 GPa (orthorhombic phase). In addition, a thorough investigation of the $\text{Fd}\bar{3}\text{m}$ phase ensures their existence at ambient conditions [18]. The nanoparticles of ZnCr_2S_4 are fabricated by mechanical alloying method and investigated the magnetism with effective magnetic moment $m_{\text{eff}} = 2.089 \text{ mB/f.u}$ and short-range magnetic interaction [19]. The single crystal Ta-doped ZnCr_2Se_4 are prepared by vapor transport method to study the impact on thermodynamic, magnetic, and structural properties. The small doping of Ta changes the direct magnetic interaction and transport behavior [20]. The theoretical study on these has not been done. Therefore, we have explored the ZnX_2Se_4 ($\text{X} = \text{Ti, V, Cr}$) theoretically, which provides evidence of the researcher's realization of applications of these compounds. The aim of study is the reporting of room temperature ferromagnetism due to exchange mechanism of electron spin rather than clustering effects of magnetic elements and effect of transport parameters on spintronic devices. The findings of integer magnetic moment and complete spin polarization increases their importance for spintronics. Moreover, a high value of power factor is found for ZnV_2Se_4 .

2. Method of Calculations

DFT calculations provide an efficient approach to compute the properties of the materials before realizing their applications for experimental analysis. The DFT has proven to be one of the most accurate theories for the calculation of the electronic structure of solids [21]. Here, WEIN2K software, which works according to full potential linearized augmented plane wave (FP-LAPW) is incorporated for calculations [13,14]. The optimization of energy

of electrons involves the calculation of eigen value as well as eigen function of Kohn–Sham expressions. To probe the ground state potential and mechanical properties, the Generalized Gradient Approximation (GGA) was employed. The calculation of band gap was performed based on modified Becke–Johnson functional of Koller et al. 2012 [22] which give the value of band gap close to the experimental value. The self-consistent converged values of c are calculated by:

$$V_{x1\sigma}^{mBJ}(r) = cV_{x1\sigma}^{BR}(r) + (3c - 2) \frac{1}{\pi} \frac{\sqrt{5}}{12} \frac{\sqrt{2t_{\sigma}(r)}}{\rho_{\sigma}(r)} \quad (1)$$

where density of the state is shown by $\rho_{\sigma}(r)$, K.E density is shown by $t_{\sigma}(r)$ and $V_{x1\sigma}^{BR}(r)$ is Becke Roussel potential (V^{BR}) and C can be calculated as:

$$c = \alpha + \left(\beta \frac{1}{V_{cell}} \int d^3r \left(\frac{|\nabla\rho(r)|}{\rho(r)}\right)\right) \quad (2)$$

where α and β behaves as free parameters into WIEN2K code, $\alpha = -0.012$ and $\beta = 1.023 \text{ Bohr}^{1/2}$.

To avoid the overlapping of core with the interstitial regions, the core region is described by the product of radial and harmonic function while interstitial region is described by the plane wave basis. Here we treated the valence states as scalar relativistic while the core region was fully relativistic. Inside the interstitial region, the cut of point of plane wave was adjusted by setting the value of $R_{MT} \times K_{max}$. In present case the value of this product is set 8. Here, R_{MT} represents the smallest value of muffin-tin radius. Inside the sphere, the expansion of spherical harmonic is controlled by the value of angular momentum l_{max} (10) while charge expansion is controlled by the value of G_{max} (18). The SCF was run until the difference between two successive measurements became less than 10^{-2} mRy. For the computation of thermoelectric properties, we need a dense mesh; therefore, we increased the number of k-points to 2000. Finally, thermoelectric parameters were computed using BoltZTraP code based on semi-classical Boltzmann equations [23].

3. Results and Discussion

3.1. Structure Behavior and Thermodynamically Stability

The structure of cubic unit cell of spinel chalcogenides ZnX_2Se_4 ($X = \text{Ti, V, Cr}$) constructed using VESTA software is shown in Figure 1. This unit cell was optimized in WIEN2K software by giving information on space group ($Fd3m$) and atomic position. The observed lattice constant (a_0), Bulk modulus (B_0), Cohesive energy (E_{coh}), Formation energy, (ΔH_f) and Curie Temperature T_c (K) for these compositions ZnX_2Se_4 ($X = \text{Ti, V, Cr}$) are presented in Table 1. The lattice constant decreases from Ti to V and Cr. This decrease in value of lattice constant is attributed to the decreases of ionic radii of Ti (0.67\AA), V (0.64\AA) and Cr (0.61\AA) [19].

Table 1. The computed $a(\text{\AA})$: Lattice constant, $B(\text{GPa})$: Bulk modulus, E_{coh} : Cohesive energy, ΔH_f (eV): Formation energy and T_c (K): Curie temperature of ZnX_2Se_4 ($X = \text{Ti, V, Cr}$).

Composition	a (\AA)	B (GPa)	E_{coh}	ΔH_f (eV)	T_c (K)
ZnX_2Se_4					
X = Ti	10.69	69.81	4.20	−1.69	250
X = V	10.61	75.48	3.18	−1.32	290
X = Cr	10.57, 10.48 [24]	78.40	2.70	−1.21	305

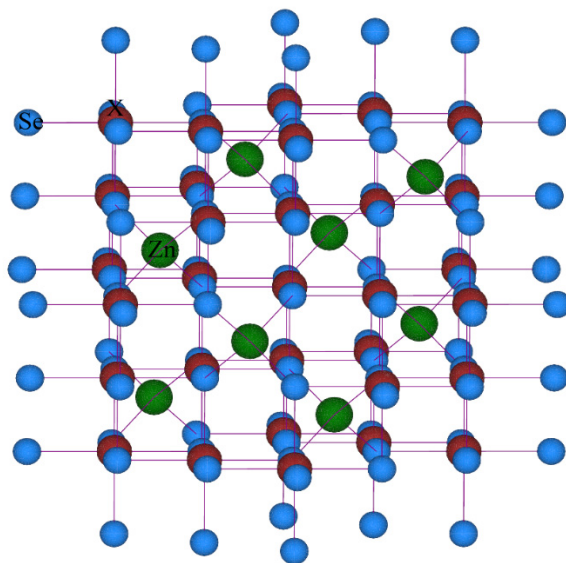


Figure 1. The crystal structure of ZnX_2Se_4 ($X = Ti, V, Cr$) formed by VESTA Software.

Stiffness of any material is one of the important factors, which determines its mechanical strength. The stiffness of the material is measured in terms of Bulk modulus (B_0) when Ti is substituted with V and Cr (See Table 1). This increase in the value of B_0 is credited to the increase in number of d -shell electrons from Ti to Cr. To ensure, in which phase compounds are more stable, their energy volume curves are plotted in ferromagnetic and antiferromagnetic phases separately and positive value of energy difference ($\Delta E = E_{AFM} - E_{FM}$) indicated that these compositions are more stable in the FM state than in the AFM state as shown in Figure 2. To further ensure the stability of the FM state, the formation energy is calculated by the following expression:

$$\Delta H_f = E_{Total}(Zn_l Se_n) - lE_{Zn} - mE_X - nE_{Se} \quad (3)$$

where $E_{Total}(Zn_l X_m Se_n)$ is the total energy of the ZnX_2Se_4 ($X = Ti, V, Cr$) chalcogenides, E_{Zn} , E_X and the E_{Se} gives energies of individual elements. The negative value of this formation energy assures the stability of these materials (See Table 1). It is evident from formation energy that Ti based composition is most stable. Cohesive energy also measures the stability of materials which is computed by relation

$$\Delta E_{coh} = aE_X^{atom} + bE_{Zn}^{atom} + cE_{Se}^{atom} - E_{Total}(Zn, X, Se) \quad (4)$$

Here $E_{Total} = (Zn_a X_b Se_c)$ is the total energy of compounds and E_X^{atom} , E_{Zn}^{atom} and E_{Se}^{atom} are energies of individual atoms. The cohesive energies of ternary compounds are larger than their binary counterparts, which shows the compounds are thermodynamically stable [25].

The curie temperature (T_c) is the important factor which disturb experimental fabrication for storage devices. The T_c is by formula, $T_c = 2\Delta E/3Xk_B$. Where k_B and X are Boltzmann constant and the content of doping elements ($X = Ti, V, Cr$), respectively [26]. The calculated values of T_c for ZnX_2Se_4 are shown in Table 1. The $ZnCr_2Se_4$ has room temperature ferromagnetism.

The higher value of T_c for Cr ($3.88\mu_B$) is due to its higher magnetic moment than V ($2.83\mu_B$) and Ti ($1.73\mu_B$). Therefore, the above prediction of RT ferromagnetism makes these alloys a potential applicant for spintronics.

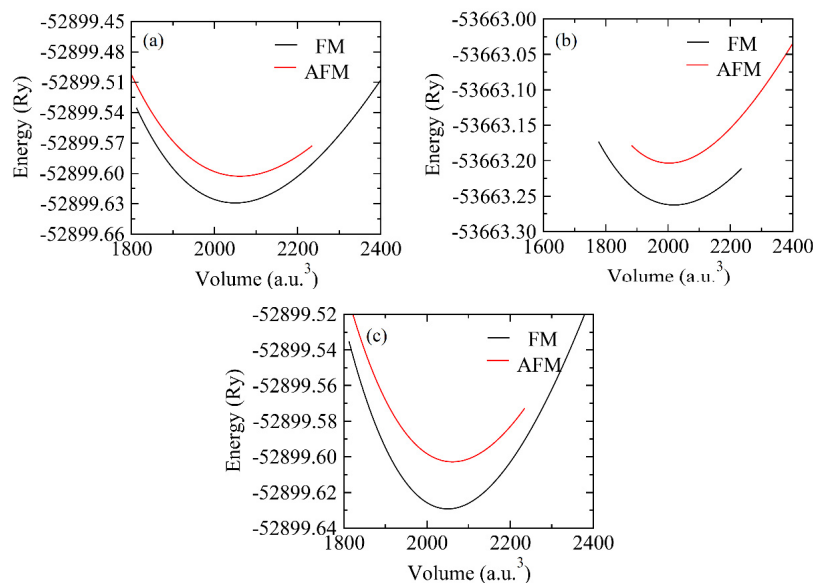


Figure 2. The optimization plots of (a) ZnTi₂Se₄, (b) ZnV₂Se₄, (c) ZnCr₂Se₄ in antiferromagnetic (AFM) and ferromagnetic (FM) phases.

3.2. Band Structure and Density of States

The spin polarization is calculated from the band structure of ZnX₂Se₄ (X = Ti, V, Cr) at the equilibrium lattice constants along different symmetry directions in first Brillion zone. The compounds in spin-up configuration reveal that the valence band maxima and conduction band minima lie at different symmetry points of the Brillion zone and some of the states of valence band cross the fermi level which exposed the metallic nature in this configuration. In addition, when band structure in spin-down channel is plotted it exhibited the direct bandgap semiconducting nature where valence band maxima and conduction band minima lie at Γ -symmetry point (See Figure 3a–c). In spin down channel, the energy states lie far from fermi level, which is attributed to the strong *p-d* splitting. The ferromagnetic semiconductors have the ability to combine magnetic and semiconducting characteristics in a single device because of this splitting. Therefore, replacement of transition metals in octahedra environment of spinel chalcogenides imparts the multifunctional characteristics to these materials.

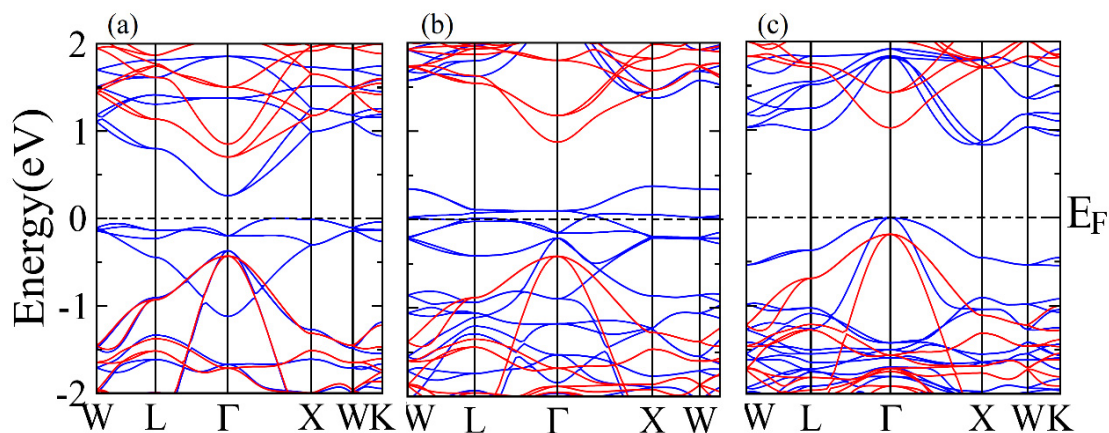


Figure 3. The band structures for up -spin channel (blue color) and down - spin channel (red color) of (a) ZnTi₂Se₄, (b) ZnV₂Se₄ and (c) ZnCr₂Se₄.

To find the origin of ferromagnetism, the total density of state (TDOS) as well as partial density of state (PDOS) for ZnX₂Se₄ (X = Ti, V, Cr) chalcogenides are shown in Figure 4a–c.

The TDOS exhibit the metallic nature in spin-up channel and semiconductor in spin-down channel. The above discussion shows that transition metals (Ti, V, Cr) doped Zn based chalcogenides have p - d exchange interaction with the valance band of host semiconductor ZnX_2Se_4 near the Fermi energy (E_F). Whenever Fermi level is controlled by impurity band gap, the p-type carrier produce ferromagnetism. The impurity explains huge exchange splitting for Ti which decrease from Ti to Cr in continues manner due to increasing number of electrons. According to the crystal field theory, the tetrahedral shape of surrounded anions produce a field, which splits the $3d$ states of (Ti, V, Cr) into $t_{2g}(d_{xy}, d_{yz}, d_{zx})$ states called bonding and $e_g(d_{x^2-y^2}, d_{z^2})$ called antibonding states [27,28]. As e_g states have low energy in contrast with t_{2g} states, therefore, the energy difference between e_g and t_{2g} in terms of crystal field energy is $E_{\text{cry}} = E_{t_{2g}} - E_{e_g}$. The large direct interchange splitting energy $\Delta_x(d)$ of $3d$ states for the transition metals ($X = \text{Ti, V, Cr}$) surpasses crystal field energy ($\Delta_x(d) > E_{\text{cry}}$), which induced ferromagnetism as shown in Table 2. Furthermore, d -states of Cr and V atoms are observed to exist at valance band maxima. For Cr doped ZnX_2Se_4 alloys, the bonding state e_g do not contribute in hybridization process due to six unpaired electrons. While Ti has two unpaired electrons, V has three unpaired electrons and Cr has four unpaired electrons according to electronic configurations.

Table 2. The computed (crystal field energy) $\Delta E_{\text{crystal}}$, interchange energy $\Delta_x(d)$, pd -exchange energy $\Delta_x(pd)$ and interchange constants ($N_o\alpha$ and $N_o\beta$) of ZnX_2Se_4 ($X = \text{Ti, V, Cr}$).

Composition	$(\Delta E_{\text{crystal}})$ eV	$\Delta_x(d)$ eV	$\Delta_x(pd)$ eV	$N_o\alpha$	$N_o\beta$
ZnX_2Se_4					
X = Ti	1.44	2.51	−0.338	1.041	−1.069
X = V	2.62	3.50	−0.195	0.182	0.210
X = Cr	1.69	2.08	−0.379	0.531	−0.306

Moreover, the interchange splitting energy $\Delta_x(pd)$ is calculated through the positions of anions or from band structures whose negative value suggest that the down-spin channel is much attractive as compared to the spin-up channel. Further, p - d repulsive model described the interaction between transition metals $3d$ state and anion p state that keep them away from fermi level because of large splitting into spin-down channel [29,30].

Furthermore, in accordance with the Pauli Exclusion Principle, the unpaired electrons in $3d$ states of transition metal impurity are equal to their magnetic moment. Thus, Ti, V, Cr have two, three and four unpaired electrons in $3d$ states. Therefore, Ti, V, and Cr containing spinels should have magnetic moment 2, 3 and 4 μ_B . Our computed values of magnetic moments for Ti, V, and Cr containing compounds are 2, 3 and 4 μ_B which are consistent with Pauli Exclusion Principle and show the accuracy of our computed results (See Table 3) [31,32]. The Cr has maximum value of magnetic moment and Ti has least value in studied transition metal doped semiconductors. Additionally, the magnetism in transition metal doped semiconductors follows the Hund's rule, which explains the increase in magnetic moments because of the interaction among s , p and d states. The transition metal impurities (Ti, V, Cr) induce magnetic moments induced at Zn and X, Se sites of host semiconductors. Moreover, knowledge of changes at valance edge is essential to find the origin of ferromagnetism. The mean field theory describes the band variation in terms of Hamiltonian, such as $H = N_o\beta$. Here, N_o is cation contribution and β is the p - d interchange integral. The Se behaves as hole carrier spin and X is impurity spin. This Hamiltonian is dependent on band disturbance that is calculated through the Kondo relations and can be defined in terms of interchange constants $N_o\alpha$ and $N_o\beta$ that are calculated from conduction band edge splitting as well as valance band edge splitting by using the following relation [33–36]:

Table 3. The computed magnetic moment of whole composition and at Zn, X = Ti, V, Cr and Se sites of ZnX_2Se_4 (X = Ti, V, Cr).

Compound	Magnetic Moments (in Terms of Bohr Magnetron, μ_B)			
	Total	Zn-Site	X-Site	S/Se-Site
ZnX_2Se_4				
X = Ti	2.000	0.017	0.875	−0.015
X = V	3.000	0.008	1.964	−0.068
X = Cr	4.000, 5.47 [24]	0.004	2.970	−0.057

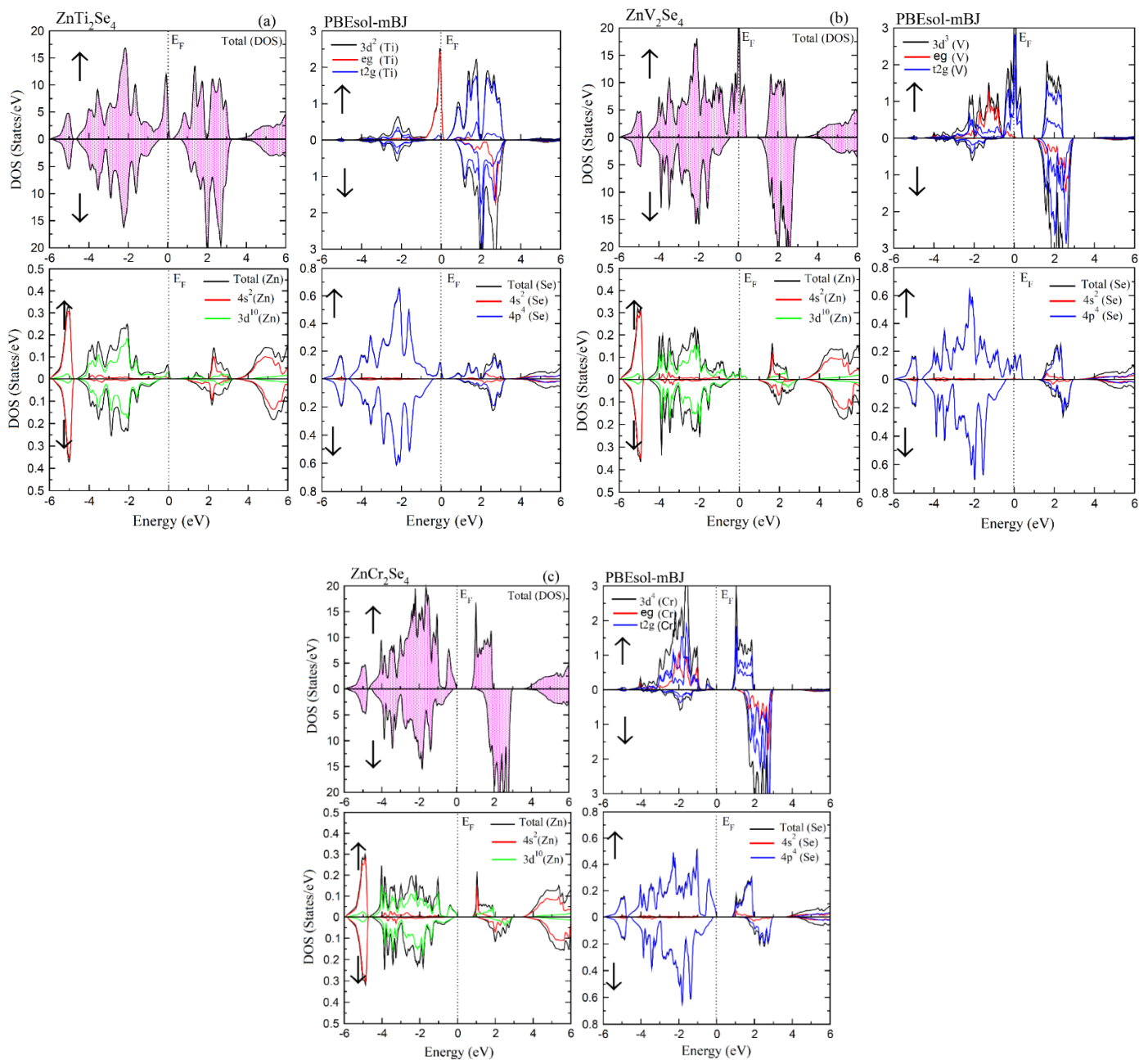


Figure 4. (a) The total DOS of $ZnTi_2Se_4$ and PDOS of Zn, Ti, S formed by PBEsol-mBJ; (b) the total DOS of ZnV_2Se_4 and PDOS of Zn, V, S formed by PBEsol-mBJ; And (c) the total DOS of $ZnCr_2Se_4$ and PDOS of Zn, Cr, S formed by PBEsol-mB.

$$N_{O\alpha} = \frac{\Delta E_C}{x\langle S \rangle} \text{ and } N_{O\beta} = \frac{\Delta E_V}{x\langle S \rangle} \quad (5)$$

where, x is the concentration of X ions and $\langle S \rangle$ represents the mean value of the magnetic moment. It is obvious that, $s-d$ as well as $p-d$ mixture are ferromagnetic for the half metallic compounds (Ti, V, Cr). In addition, the more negative value of $N_{O\beta}$ shows the ferromagnetism in transition metal doped ($X = \text{Ti, V, Cr}$) Zn based alloys is decreases the energy of the system to stabilize ferromagnetism (See Table 2).

The Pauli exclusion principle states that a single quantum state cannot be filled with two identical fermions. Depending upon the number of unpaired electrons in the outermost shell, the magnetic moment of Ti is $2\mu_B$, V is $3\mu_B$ and Cr is $4\mu_B$. This increase in magnetic moment is due to increase in unpaired electrons in the outer shells whose integral values ensure the complete spin polarization (See Table 3) [37–40].

3.3. Transport Properties

The thermoelectric measurement converts the directly heat energy into electrical energy by thermoelectric generators. Investigation of transport properties usually involve the measurement of electrical conductivity (σ), thermal conductivity (κ), Seebeck coefficient (S), power factor (PF) and figure of merit (ZT), which quantify the response of materials towards thermoelectric applications [41–45]. Here we have computed these properties using BoltzTraP code. The thermal conductivity has two parts, i.e., electron (k_{el}) and phonon (k_{ph}). Here we incorporated the electronic part only because this code could not work for phonon calculations. In addition, this code works well for metals having an excess number of electrons which suppress the lattice contribution in thermal conductivity. The density functional theory perturbation (DFTP) approach is considered more effective to incorporating the phonon part in conductivity, hence the reason for only reporting the electronic part. Figure 5a shows the variation of σ in the temperature range of 0–400 K. For ZnTi_2Se_4 , it slightly increases in the lower T range ($T < 350$ K) and become almost constant when temperature increases from 350 K. The ZnV_2Se_4 has maximum value of σ which is attributed to the odd number of electrons present in $3d$ states of V [46–50]. The ZnCr_2Se_4 has a least value of σ which linearly increased with temperature.

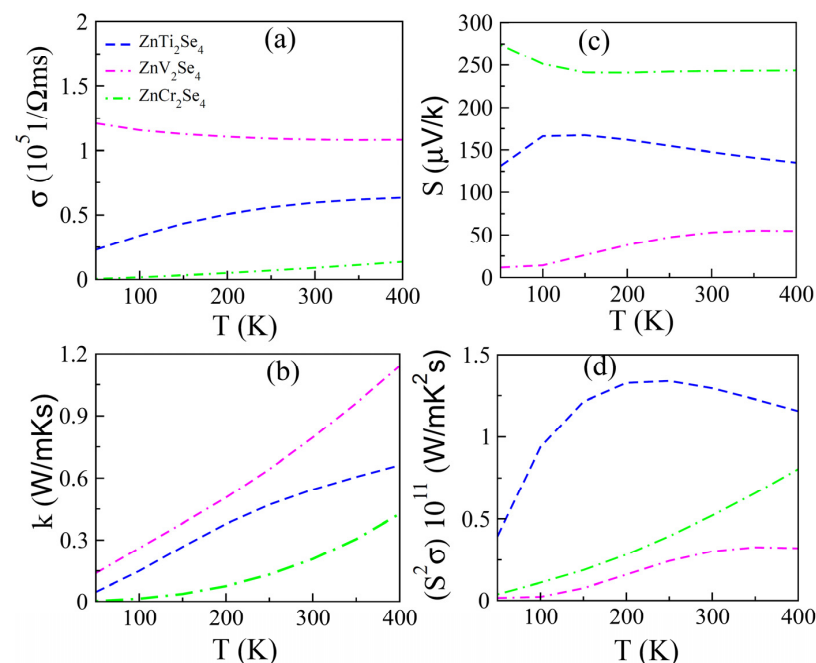


Figure 5. (a) σ , (b) k , (c) S and (d) σS^2 of ZnX_2Se_4 ($X = \text{Ti, V, Cr}$) computed by Boltz TraP code.

Seebeck coefficient (S) measures the potential gradient developed across two dissimilar materials when these materials meet each other. The variation in S with temperature is shown in Figure 5c in the temperature range 0–400 K. For all compositions, S is positive which reveal the fact that in these compositions, the majority charge carries are holes. The S is maximum for Cr and minimum for V containing compositions. At 400 K, S is 130 $\mu\text{V}/\text{K}$ for ZnTi_2Se_4 , 57 $\mu\text{V}/\text{K}$ for ZnV_2Se_4 and 245 $\mu\text{V}/\text{K}$ for ZnCr_2Se_4 . The product of σ and S^2 determine another important factor called power factor (PF), which verify the thermoelectric strength of the material [51]. Figure 5d shows how the power factor varies in the temperature range 0–400 K. The PF is maximum for ZnTi_2Se_4 and minimum for ZnV_2Se_4 . Based on this observation, we can claim that ZnTi_2Se_4 is the most suitable candidate among the present compounds for thermoelectric applications.

4. Conclusions

In summary, half metallic ferromagnetism and transport behavior of ZnX_2Se_4 ($X = \text{T}, \text{V}, \text{Cr}$) have been comprehensively analyzed. The more energy released in ferromagnetic state than in anti-ferromagnetic state confirms their stability in FM states, which is further ensured by negative formation energy and positive values of cohesive energy. The Curie temperatures of Ti, V and Cr based chalcogenides are 250, 290 and 305 K. The integer magnetic moment and band structures show the 100% spin polarization. The ferromagnetism is explored by strong hybridization, and greater values of exchange energies than crystal field energies. Moreover, negative values of $N_0\beta$ and pd coupling energy lower the energy of the spin-orbit coupling system to stabilize ferromagnetism and ensures ferromagnetism due to exchange of electrons rather than clustering of magnetic ions. Thermoelectric behavior shows the ZnTi_2Se_4 has large value of power factor, which increases its thermoelectric performance.

Author Contributions: The authors M.A.-Q., Z.I.Z., N.Y.M., S.H.A. and M.A.A. write the manuscript draft and proofread the whole manuscript. G.M.M., N.M., S.B., Q.M. and A.M. computed the results compiled and analyzed. All authors have read and agreed to the published version of the manuscript.

Funding: The members of the Materials Science and Engineering Group would like to express their gratitude for Taif University, KSA for funding this project under the grant no. 1-439-6068.

Institutional Review Board Statement: Not applicable.

Informed Consent Statement: Not applicable.

Data Availability Statement: Data will be available on request.

Acknowledgments: The members of the Materials Science and Engineering Group would like to express their gratitude for Taif University, KSA for funding this project under the grant no. 1-439-6068.

Conflicts of Interest: Authors have not any conflict of interest.

References

1. Cid, A.; Simal-Gandara, J. Synthesis, characterization, and potential applications of transition metal nanoparticles. *J. Inorg. Organomet. Polym. Mater.* **2020**, *30*, 1011–1032. [[CrossRef](#)]
2. Alkathy, M.S.; Lente, M.H.; Eiras, J. Bandgap narrowing of $\text{Ba}_{0.92}\text{Na}_{0.04}\text{Bi}_{0.04}\text{TiO}_3$ ferroelectric ceramics by transition metals doping for photovoltaic applications. *J. Mater. Chem. Phys.* **2021**, *257*, 123791. [[CrossRef](#)]
3. Aravindh, S.A.; Schwingenschloeg, U.; Roqan, I.S. Ferromagnetism in Gd doped ZnO nanowires: A first principles study. *J. Appl. Phys.* **2014**, *116*, 233906. [[CrossRef](#)]
4. Zhang, Z.; Schwingenschloeg, U.; Roqan, I.S. Possible mechanism for d 0 ferromagnetism mediated by intrinsic defects. *RSC Adv.* **2014**, *4*, 50759–50764. [[CrossRef](#)]
5. Roqan, I.S.; Venkatesh, S.; Zhang, Z.; Hussain, S.; Bantounas, I.; Franklin, J.B.; Flemban, T.H.; Zou, B.; Lee, J.-S.; Schwingenschloeg, U.; et al. Obtaining strong ferromagnetism in diluted Gd-doped ZnO thin films through controlled Gd-defect complexes. *J. Appl. Phys.* **2015**, *117*, 073904. [[CrossRef](#)]
6. Mahmood, Q.; Haq, B.U.; Rashid, M.; Noor, N.; AlFaify, S.; Laref, A. First-principles study of magnetic and thermoelectric properties of SnFe_2O_4 and SnCo_2O_4 spinels. *J. Solid State Chem.* **2020**, *286*, 121279. [[CrossRef](#)]

7. Mahmood, Q.; Noor, N.; Jadan, M.; Addasi, J.S.; Mahmood, A.; Ramay, S.M. First-principle investigation of ferromagnetism and thermoelectric characteristics of MgCr_2X_4 ($\text{X} = \text{S}, \text{Se}$) spinels. *J. Solid State Chem.* **2020**, *285*, 121261. [[CrossRef](#)]
8. Zhang, R.L.; Damewood, L.; Fong, C.Y.; Yang, L.H.; Peng, R.; Felser, C. A half-metallic half-Heusler alloy having the largest atomic-like magnetic moment at optimized lattice constant. *AIP Adv.* **2016**, *6*, 115209. [[CrossRef](#)]
9. De Groot, R.A.; Mueller, F.M.; Van Engen, P.G.; Buschow, K.H.J. New Class of Materials: Half-Metallic Ferromagnets. *Phys. Rev. Lett.* **1983**, *50*, 2024. [[CrossRef](#)]
10. Muz, I.; Goktaş, F.; Kurban, M. 3d-transition metals (Cu, Fe, Mn, Ni, V and Zn)-doped pentacene π -conjugated organic molecule for photovoltaic applications: DFT and TD-DFT calculations. *Theor. Chem. Acc.* **2020**, *139*, 23. [[CrossRef](#)]
11. Elhorri, A.M. Theoretical study of new push–pull molecules based on transition metals for NLO applications and determination of ICT mechanisms by DFT calculations. *J. Theo. Comp. Chem.* **2020**, *19*, 2050026. [[CrossRef](#)]
12. Mahmood, Q.; Hassan, M.; Bhamu, K.; Yaseen, M.; Ramay, S. Density functional theory-based study of the magnetic and optical properties of PbMO_3 ($\text{M} = \text{Cr}, \text{Fe}$) using the modified Becke Johnson mBJ functional. *J. Phys. Chem. Solids* **2021**, *158*, 110225. [[CrossRef](#)]
13. Gueddida, S.; Lebegue, S.; Badawi, M. Interaction between transition metals (Co, Ni, and Cu) systems and amorphous silica surfaces: A DFT investigation. *Appl. Surf. Sci.* **2020**, *533*, 147422. [[CrossRef](#)]
14. Khandy, S.A.; Chai, J.-D. Novel half-metallic L_{21} structured full-Heusler compound for promising spintronic applications: A DFT-based computer simulation. *J. Magn. Magn. Mater.* **2019**, *487*, 165289. [[CrossRef](#)]
15. Kapuria, N.; Ghorpade, U.V.; Zubair, M.; Mishra, M.; Singh, S.; Ryan, K.M. Metal chalcogenide semiconductor nanocrystals synthesized from ion-conducting seeds and their applications. *J. Mater. Chem. C* **2020**, *8*, 13868–13895. [[CrossRef](#)]
16. Cui, X.; Soon, A.; Phillips, A.; Zheng, R.; Liu, Z.; Delley, B.; Ringer, S.; Stampfl, C. First principles study of 3d transition metal doped Cu_3N . *J. Magn. Magn. Mater.* **2012**, *324*, 3138–3143. [[CrossRef](#)]
17. Vaipolin, A.A.; Nikolaev, Y.A.; Polushina, I.K.; Rud', V.Y.; Rud', Y.V.; Terukov, E.I.; Fernelius, N. Fabrication and Properties of ZnFe_2S_4 Single Crystals and Structures Based on Them. *Semiconductors* **2003**, *37*, 656–660. [[CrossRef](#)]
18. Efthimiopoulos, I.; Lochbiler, T.; Tsurkan, V.; Loidl, A.; Felea, V.; Wang, Y. Structural Behavior of ZnCr_2S_4 Spinel under Pressure. *J. Phys. Chem. C* **2017**, *121*, 769–777. [[CrossRef](#)]
19. Gudwański, A.; Malicka, E.; Groń, T.; Karolus, M.; Oboz, M.; Sawicki, B.; Nowok, A.; Pawlus, S.; Duda, H. Electrical and magnetic properties of ZnCr_2S_4 nanoparticles. *J. Alloy. Compd.* **2021**, *861*, 157973. [[CrossRef](#)]
20. Jendrzewska, I.; Gro, T.; Kwapulinski, P.; Kusz, J.; Pietrasik, E.; Goryczka, T.; Sawicki, B.; Slebarski, A.; Fijalkowski, M.; Jampilek, J.; et al. Study of the Structure, Magnetic, Thermal and Electrical Characterization of ZnCr_2Se_4 : Ta Single Crystals Obtained by Chemical Vapour Transport. *Materials* **2021**, *14*, 2749. [[CrossRef](#)]
21. Elahmar, M.H.; Rached, H.; Rached, D. The half metallic feature at high temperature of the novel half-Heusler alloys and their [100] oriented layered superlattices: A DFT investigations. *Mater. Chem. Phys.* **2021**, *267*, 124712. [[CrossRef](#)]
22. Koller, D.; Tran, F.; Blaha, P. Improving the modified Becke-Johnson exchange potential. *Phys. Rev. B* **2012**, *85*, 155109. [[CrossRef](#)]
23. Madsen, G.K.H.; Singh, D.J. A code for calculating band-structure dependent quantities. *Comput. Phys. Commun.* **2006**, *175*, 67–71. [[CrossRef](#)]
24. Jendrzewska, I.; Zajdel, P.; Maciążek, E.; Sozańska, M. Growth, structure and magnetic properties of ZnCr_2Se_4 -single crystals doped by dysprosium. *J. Cryst. Growth* **2014**, *401*, 697–701. [[CrossRef](#)]
25. Shakerzadeh, E. Electro-optical properties of bowl-like B36 cluster doped with the first-row transition metals: A DFT insight. *Phys. E Low-Dimens. Syst. Nanostruct.* **2019**, *114*, 113599. [[CrossRef](#)]
26. Zhang, R.; Wang, Q.; Liang, J.; Li, Q.; Dai, J.; Li, W. Optical properties of N and transition metal R ($\text{R} = \text{V}, \text{Cr}, \text{Mn}, \text{Fe}, \text{Co}, \text{Ni}, \text{Cu}$, and Zn) codoped anatase TiO_2 . *Phys. B Condens. Matter* **2012**, *407*, 2709–2715. [[CrossRef](#)]
27. Guo, J.; Liao, X.; Lee, M.-H.; Hyett, G.; Huang, C.-C.; Hewak, D.W.; Mailis, S.; Zhou, W.; Jiang, Z. Experimental and DFT insights of the Zn-doping effects on the visible-light photocatalytic water splitting and dye decomposition over Zn-doped BiOBr photocatalysts. *Appl. Catal. B Environ.* **2019**, *243*, 502–512. [[CrossRef](#)]
28. She, A.Q.; Gupta, D.C. Comprehensive DFT investigation of transition-metal-based new quaternary Heusler alloys CoNbMnZ ($\text{Z} = \text{Ge}, \text{Sn}$): Compatible for spin-dependent and thermoelectric applications. *RSC Adv.* **2020**, *10*, 43870–43881.
29. Laref, A.; Madkhali, N.; Alqahtani, H.; Wu, X.; Laref, S. Electronic structures and optical spectroscopies of 3d-transition metals-doped melanin for spintronic devices application. *J. Magn. Magn. Mater.* **2019**, *491*, 165513. [[CrossRef](#)]
30. Woods-Robinson, R.; Han, Y.; Zhang, H.; Ablekim, T.; Khan, I.; Persson, K.A.; Zakutayev, A. Wide band gap chalcogenide semiconductors. *Chem. Rev.* **2020**, *120*, 4007–4055. [[CrossRef](#)] [[PubMed](#)]
31. Islam, M.; Sarker, M.; Nakamura, T.; Khan, M.; Khan, F.; Rahman, M.; Sato, S. Structural, electronic and magnetic properties of L_{10} ordered CoPt nanoparticles: An experimental and DFT study. *Mater. Chem. Phys.* **2021**, *269*, 124727. [[CrossRef](#)]
32. Hossain, A.; Sarker, M.; Khan, M.; Rahman, M. Spin effect on electronic, magnetic and optical properties of spinel CoFe_2O_4 : A DFT study. *Mater. Sci. Eng. B* **2020**, *253*, 114496. [[CrossRef](#)]
33. Jia, T.-T.; Feng, Z.; Guo, S.; Zhang, X.; Zhang, Y. Screening Promising Thermoelectric Materials in Binary Chalcogenides through High-Throughput Computations. *ACS Appl. Mater. Interfaces* **2020**, *12*, 11852–11864. [[CrossRef](#)]
34. Vu, D.V.; Le, D.H.; Nguyen, C.X.; Trinh, T.Q. Comparison of structural and electric properties of ZnO-based n-type thin films with different dopants for thermoelectric applications. *J. Sol-Gel Sci. Technol.* **2019**, *91*, 146–153.

35. Zahra, R.; Jacob, J.; Bano, N.; Ali, A.; Mahmood, K.; Ikram, S.; Hussain, S. Effect of secondary phases on the thermoelectric properties of Zn_2GeO_4 nanocrystals grown by thermal evaporation on Au coated Si substrate. *Phys. B Condens. Matter* **2019**, *564*, 143–146. [[CrossRef](#)]
36. Seh, A.Q.; Gupta, D.C. Exploration of highly correlated Co-based quaternary Heusler alloys for spintronics and thermoelectric applications. *Int. J. Energy Res.* **2019**, *43*, 8864–8877. [[CrossRef](#)]
37. Huma, M.; Rashid, M.; Mahmood, Q.; Algrafy, E.; Kattan, N.A.; Laref, A.; Bhatti, A.S. Physical properties of lead free double perovskites A_2SnI_6 (A = Cs, Rb) using ab-initio calculations for solar cell applications. *Mater. Sci. Semicond. Process.* **2012**, *121*, 105313. [[CrossRef](#)]
38. Sabir, B.; Murtaza, G.; Mahmood, Q.; Ahmad, R.; Bhamu, K. First principles investigations of electronics, magnetic, and thermoelectric properties of rare earth based PrYO_3 (Y = Cr, V) perovskites. *Curr. Appl. Phys.* **2017**, *17*, 1539–1546. [[CrossRef](#)]
39. Mahmood, Q.; Hassan, M.; Noor, N.A. Systematic study of room temperature ferromagnetism and optical response of $\text{Zn}_{1-x}\text{TM}_x\text{S}/\text{Se}$ (TM = Mn, Fe, Co, Ni) ferromagnets: First principle approach. *J. Phys. Cond. Matt. Phys.* **2016**, *28*, 506001. [[CrossRef](#)] [[PubMed](#)]
40. Zhang, C.W.; Yan, S. Nonvolatile, reversible electric-field controlled switching of remanent magnetization in multifunctional ferromagnetic/ferroelectric hybrids. *J. Appl. Phys.* **2010**, *107*, 043913. [[CrossRef](#)]
41. Saini, H.S.; Singh, M.; Reshak, A.H.; Kashyap, M.K. A first principles study of half-metallic ferromagnetism in $\text{In}_{1-x}\text{Ti}_x\text{P}$ ($x = 0.06$) diluted magnetic semiconductor. *J. Magn. Mater.* **2013**, *331*, 130007.
42. Bai, Z.Q.; Lu, Y.H.; Shen, L.; Ko, V.; Han, G.C.; Feng, Y.P. Transport properties of high-performance all-Heusler $\text{Co}_2\text{CrSi}/\text{Cu}_2\text{CrAl}/\text{Co}_2\text{CrSi}$ giant magnetoresistance device. *J. Appl. Phys.* **2012**, *111*, 093911. [[CrossRef](#)]
43. Choi, H.C.; Shim, J.H.; Min, B.I. Electronic structures, and magnetic properties of spinel $\text{Zn Mn}_2\text{O}_4$ under high pressure. *Phys. Rev. B* **2006**, *74*, 172103. [[CrossRef](#)]
44. Leoni, S.; Yaresko, A.N.; Perkins, N.; Rosner, H.; Craco, L. Orbital-spin order and the origin of structural distortion in MgTi_2O_4 . *Phys. Rev. B* **2008**, *78*, 125105. [[CrossRef](#)]
45. Walsh, A.; Wei, S.-H.; Yan, Y.; Al-Jassim, M.M.; Turner, J.A.; Woodhouse, M.; Parkinson, B.A. Structural, magnetic, and electronic properties of the Co-Fe-Al oxide spinel system: Density-functional theory calculations. *Phys. Rev. B* **2007**, *76*, 165119. [[CrossRef](#)]
46. Dalpian, G.M.; Wei, S.H. Electron-mediated ferromagnetism, and negative s–d exchange splitting in semiconductors. *Phys. Rev. B* **2006**, *73*, 245204. [[CrossRef](#)]
47. Mahmood, Q.; Hassan, M.; Ahmad, S.; Bhamu, K.; Mahmood, A.; Ramay, S.M. Study of electronic, magnetic, and thermoelectric properties of AV_2O_4 (A = Zn, Cd, Hg) by using DFT approach. *J. Phys. Chem. Solids* **2019**, *128*, 283–290. [[CrossRef](#)]
48. Mahmood, Q.; Hassan, M.; Algrafy, E.; Haq, B.U.; Kattan, N.A.; Murtaza, G.; Laref, A. Theoretical investigations of optoelectronic and thermoelectric properties of the XIn_2O_4 (X = Mg, Zn, Cd) spinel oxides. *J. Phys. Chem. Solids* **2020**, *144*, 109481. [[CrossRef](#)]
49. Liu, C.; Morelli, D.T. The Theoretical Investigation of Electronic, Magnetic, and Thermoelectric Behavior of LiZ_2O_4 (Z = Mn, Fe, Co, and Ni) by Modified Becke and Johnson Approach. *J. Elect. Mat.* **2011**, *40*, 678. [[CrossRef](#)]
50. Singh, S.; Maurya, R.K.; Pandey, S.K. Investigation of thermoelectric properties of ZnV_2O_4 compound at high temperatures. *J. Phys. D Appl. Phys.* **2016**, *49*, 425601. [[CrossRef](#)]
51. Ramachandran, T.; Rajeevan, N.E.; Pradyumnan, P.P. Enhanced Thermoelectric Properties of BiCoO_3 by Nickel Substitution. *Mater. Sci. Appl.* **2013**, *4*, 816.